FULL PAPER

ADVANCED
MATERIALS
TECHNOLOGIE

www.advmattechnol.d

Check for
updates

Folding and Bending Planar Coils for Highly Precise Soft Angle Sensing

Hongbo Wang,* Massimo Totaro, Selvaraj Veerapandian, Muhammad Ilyas, Minsik Kong, Unyong Jeong, and Lucia Beccai*

Sensors detecting angles created by deformable structures play an increasing role in soft robotics and wearable systems. However, the typical sensing method based on strain measurement strongly depends on the viscoelastic behaviors of soft substrates and on the location of sensors that affect the sensing reliability. In this work, the changes in magnetic field coupling produced in space by planar coil deformation are investigated, for implementing a new direct transduction strategy, the soft inductive angle sensing (SIAS). A numerical analysis tool is developed for rigorously studying the inductance variations resulting from planar coils' bending, folding, and folding with a small arc. Copper or liquid metal coils, having different shapes, pitches, and sizes are built and characterized. Results show that the SIAS is hysteresis-free, velocity-independent, highly sensitive, ultrastable, and with fast response, guaranteeing highly precise (0.1° incremental folding angle change) and reliable measurements. It is insensitive to coil materials and to behavior of embedding soft materials, and scalable (across 10 times scale). The SIAS is adopted in three case studies (a self-sensing origami, a sensorized soft pneumatic actuator, and a wearable sensor) to highlight its low implementation complexity, high-performance, and versatility, providing some insights on the enormous potential of this mechanism.

1. Introduction

In the last decades, remarkable progress was made in developing soft mechanical sensors[1] able to retrieve mechanical cues, such as pressure or contact, shear force, strain, bending, and twisting/rotation for various applications. Among them,

soft sensors that can measure the angle of a joint or a curved surface play an increasingly important role in applications spanning from robotics[1a] to wearable systems.[1c] Unlike their rigid counterparts, soft robots[2] can actively and passively change their shape to interact safely and effectively with humans, and are adaptable to the environment. In this context, soft angle sensing is crucial to reconstruct the body-shape for feedback control,[1a] to achieve the target morphology and adaptation. On the other hand, inspiring from the paper folding art,[3] origami robotics[4] provides a top-down approach to simplify and accelerate the robots' design and development, enabling reconfiguration and adaptation. Despite many remarkable achievements,[4,5] the majority of origami robots are operating with open-loop, on/off control, due to the posed constraints (dimension, space, weight, etc.) for sensor integration. Furthermore, soft sensors that can monitor joint angles and movements are essential components for human activity monitoring in the rapidly growing area of wearable systems[1c,6] as well.

Despite the high demands and extensive researches in applications like wearable and soft robotic systems, soft angle sensing remains less developed and not well defined. For example, some strain sensors have been demonstrated to detect the "bending" angle of human/bionic fingers.[7] However, since our fingers have rigid bones and physical joints, the finger "bending" is actually a rotation/folding movement between two bone segments, rather than pure bending. To clearly define the sensing parameters, and to make a rigorous analysis and discussion of soft angle sensors, we classify them according to two different types of deformations, namely bending and folding. Bending means that the object is curved into a portion of a circle (ring) or a cylindrical surface with constant curvature, while folding means that one part of an object is rotating with respect to the other part along a folding axis.

In literature, the majority of soft angle sensors embed strain sensitive layouts and/or materials, to detect the strain caused by the bending or folding of a soft body or flexible substrate. In the last decades, different transducer mechanisms—from capacitive,[8] resistive,[7,9] to optical,[10] etc.—have been extensively investigated together with the enabling new materials/structures

Dr. H. Wang, Dr. M. Totaro, Dr. M. Ilyas, Dr. L. Beccai
Center for Micro-BioRobotics
Istituto Italiano di Tecnologia (IIT)
Viale Rinaldo Piaggio 34, Pontedera, Pisa 56025, Italy
E-mail: hongbo.wang@iit.it; lucia.beccai@iit.it
Dr. S. Veerapandian, M. Kong, Prof. U. Jeong
Department of Materials Science and Engineering
Pohang University of Science and Technology
Cheongam-Ro 77, Namgu, Pohang, Gyeongbuk 37673, Republic of Korea

and advanced fabrication techniques, to develop high-performance, reliable, stretchable strain sensors which subsequently have been demonstrated for angle sensing in robotics and wearable systems. Notably, multiple stretchable optical waveguide-based strain sensors were integrated into a soft prosthetic hand to detect the fingers' bending angle.[10] Also, Totaro et al.[9a] presented a soft structure with bidirectional bending sensing by implanting gold nanoparticles into the elastomer surface to form a strain gauge that is sensitive to both tensile and compressive strains. Alternatively, the same authors placed a pair of textile-based capacitive strain sensors[11] on both sides of a cylindrical soft body to detect bending. Moreover, a fully integrated robotic origami[12] was developed by utilizing highly sensitive piezoresistive sensors for folding angle detection.

However, there are some limitations and drawbacks in implementing strain sensors for bending and folding angle sensing. In the case of pure bending sensing,[13] the strain sensor should be located in a position with a sufficient distance from the neutral plane of the bending, so that the strain is larger enough to be detected. Moreover, the sensor can only be placed on the stretched part of the soft body given that most stretchable strain sensors are developed to measure tensile strain rather than compression. Recently, a crack-enhanced flexible strain sensor[14] with bidirectional strain sensing capabilities and extremely high sensitivity to small strain was developed to ease these limitations. In the case of folding angle sensing in wearable systems,[6] only the surface area close to the folding axis (joint) is significantly stretched. Therefore, strain sensitive unit must be placed on the large strain area to achieve good sensitivity, and sliding or movements between the skin and the sensors could cause significant measurement errors. Moreover, it is particularly challenging to sense the folding/bending angle of flexible thin-film structures (e.g., origami,[3] printed, and flexible sensors[15]) by strain measurement,[12] given that the large strain area (the outer side of the crease) is too small to host a sensor that can detect the folding angle effectively, without impairing the folding and unfolding movement. For example, researchers have developed a bioinspired interlocked structure[15] to make flexible pressure sensor compliant, robust, sensitive, and functional at deformed state, which is also sensitive to bending. Although the presented device can be utilized as bending sensor, the pressure measurement can be easily affected by a bending/folding deformation. Hence, it is crucial to discriminate the detection of bending/folding and pressure, toward truly multimodal, flexible film sensors.

Moverover, in strain-based angle sensing, the results are often affected by the mechanical behaviors (e.g., hysteresis, viscoelasticity, etc.) of the materials used for building the soft sensors, which make it difficult to achieve accurate, stable, and fast sensing responses for feedback control in robotic applications. In addition, since most strain sensors are implemented to measure the strain of a line or a surface to obtain the angle information indirectly, local defects that originate in sensor fabrication or integration, and even inhomogeneity of the hosting structures can all introduce errors in the angle measurements. Recently, to overcome these limitations, researchers have investigated a displacement sensing approach.[16] For example, the bending curvature of a snake-like soft robot can be obtained by measuring tangential displacement between two points on the middle plane of a cylindrical body, through embedded magnets and magnetic field sensors.[16a] Similarly, light-emitting diode and photodiode

pairs[16b] have been integrated on an origami robot to detect folding angles. Nonetheless, being a point to point sensing method, the angle measurement results are highly dependent on the exact location where the components are embedded.

Among all sensing mechanisms, inductive sensing has been widely used in industry, particularly for noncontact displacement sensing[17] and nondestructive testing,[18] but not extensively studied for soft sensing systems. Recently, several inductive transduction principles have been employed for building soft sensors, varying from eddy-current effect, to magnetic reluctance, and self/mutual inductance. Pressure, shear force, and deformation were measured by exploiting the eddy-current effect,[19] and the low magnetic reluctance of magnetorheological elastomers,[20] or ferrite films.[21] Hyperelastic strain sensing was achieved by measuring the self-inductance of stretchable coils made of liquid metal traces[22] or zig-zag metal wires[23] embedded in elastomers. Helical coils, like an extensible and compressible spring, were used for detecting pneumatic artificial muscles' contraction[24] and extension[25] through inductance measurement. Moreover, helical coils made of copper-wire[26] and printed liquid metal,[27] have been also exploited for bending curvature sensing in wearables and snake-like soft robots, respectively. Both studies show promising results for angle sensing, but fabrication of helical coils and integrating them into application systems are rather complicated given its 3D structure.

Planar coils have been widely used as inductors (together with resistors and capacitors) in electronic systems, also playing an increasingly important role in wireless powering[28] and communication systems,[29] particularly in biomedical systems. In contrast to 3D coils, the planar configuration can be easily fabricated by many technologies,[30] e.g., printed-circuit boards (PCB), lithography, ink-jet/nozzle printing, screen printing, etc. Unlike rigid silicon chips, flexible and stretchable planar coils are often being implemented on curved surfaces or even being deformed during operation, in applications from implantable biomedical devices,[31] wearable systems,[21] soft robotics,[20b] to flexible sensors and electronic systems.[32] Since the inductance of a coil is determined by the geometry of the wire loops, it is well-known that it varies upon coil deformation (e.g., bending and folding). From the magnetic field energy point of view, the inductance of a planar coil decreases to zero, when it is fully folded into two overlapped halves, in which the magnet field of each half completely cancels each other. However, it remains unclear how much the inductance (i.e., the most important parameter) changes when such a planar coil is folded by a specific angle or bent to a certain curvature.

Driven by the curiosity of understanding the underlying physics of planar coil folding and bending, as well as the enormous potentials of utilizing this mechanism for building film-like soft angle sensors, our primary goal is to fill this research gap for the first time through a rigorous study. In this work, we begin by classifying the deformation of planar coils into folding and bending and investigating how the inductance changes. We develop a new numerical analysis tool to investigate the coils' inductance change due to folding, bending, and folding with a small arc (which represents the real case for physical devices). Flexible printed circuit (FPC) coils with different design parameters (shape, pitch, and size) and liquid metal (LM) coils are fabricated and characterized, then evaluated for folding and bending angle sensing. Cyclic testing shows that this new angle

sensing mechanism, i.e., the soft inductive angle sensing (SIAS), is velocity-independent, hysteresis-free, and highly repeatable. Further experiments show that the planar coil can clearly detect 0.1° incremental folding angle change. The SIAS response is extremely stable with only 0.08° drift after 10 000 cycles, and is fast enough (500 Hz sampling rate) to detect the vibration of a cantilever plate. Finally, we address some representative case studies to demonstrate applications in self-sensing origami structures, wearable sensors, and perceptive soft robotics.

2. Results and Discussion

2.1. Folding and Bending of Planar Coils

As depicted in **Figure 1**, we define the deformation of a planar coil as either folding or bending, to rigorously investigate

the consequent inductance change. Folding refers to the coils folded into two planar parts along a folding axis; while bending refers to the coil plane that is only subjected to pure bending with constant curvature (i.e., curved as a cylindrical surface).

2.1.1. Theoretical Analysis

Given that no closed-form equations can be derived to calculate the inductance of a coil in most cases, a coil made of a single-turn rectangular loop (10 × 5 mm², inset of Figure 1B; and Figure S1, Supporting Information) was investigated to understand how the inductance changes when it is folded into two equal halves (A'B'CD folded to ABQCDP). The inductance of the folded coil is the sum of self-inductance of these filaments and mutual inductance between
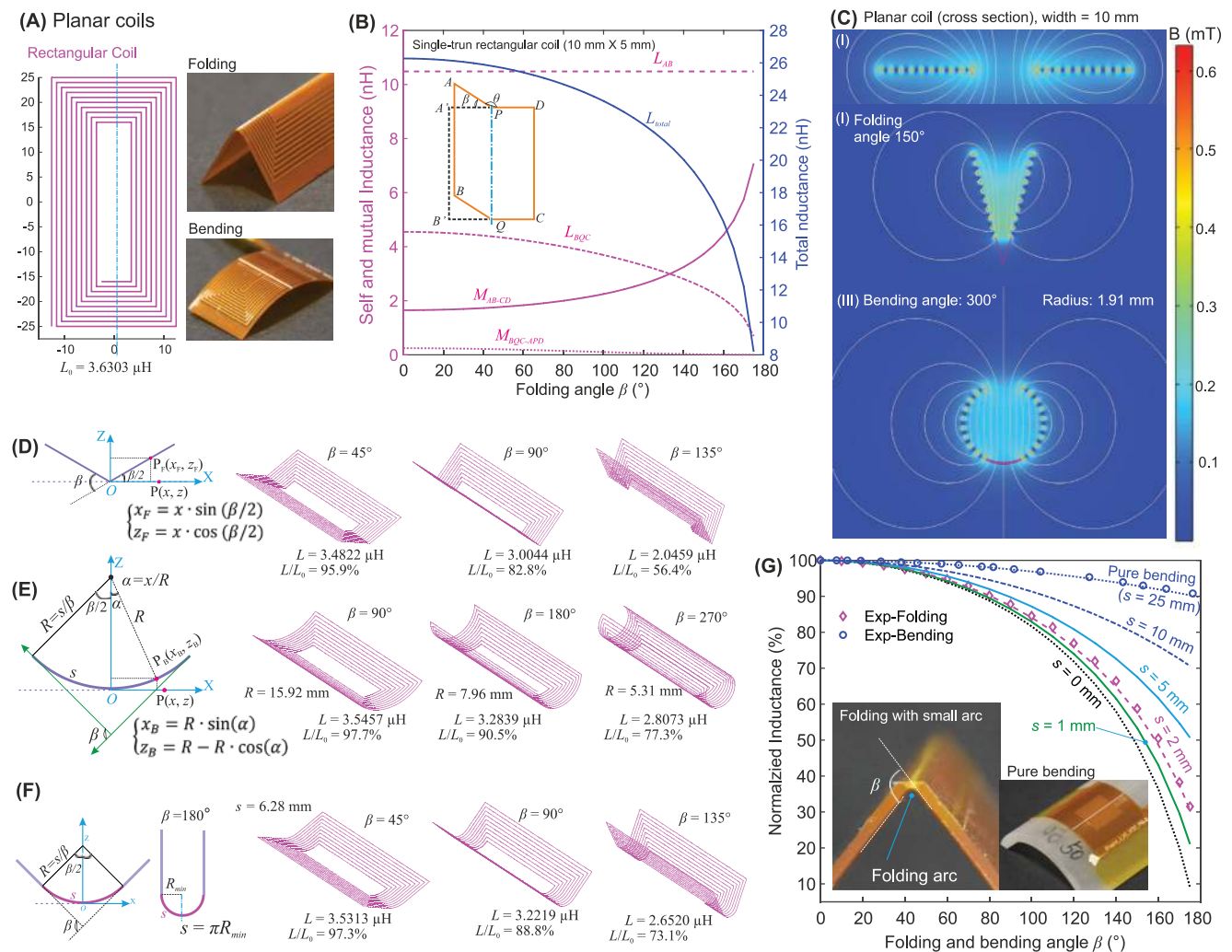

Figure 1. Folding and bending of planar coils: concept, modeling, and basic characteristics. A) Sketch of a rectangular planar coil (length: 50 mm, width: 25 mm, pitch: 1 mm, 10 turns) and images of a flexible planar coil folded into an acute angle, and bent to a cylindrical surface. B) Inductance variations of a single-turn, rectangular coil folded from 0° to 170° (length: 10 mm, width: 5 mm, folded along the length). C) Magnetic flux lines of a long rectangular planar coil (cross-section); magnetic flux when the coil is folded by 150°, and when it's bended by 300° (bending radius: 1.91 mm); D) Folding, E) Bending, and F) Folding with a small arc, of a planar coil and its inductance variations calculated through numerical analysis. G) Experimental characteristics of a rectangular coil's inductance variation caused by folding and bending, in comparison with numerical analysis results of the same coil folded with different arcs.

them: $L_{total} = 2L_{AB} + 2L_{BQC} - 2M_{AB-CD} - 2M_{BQC-APD}$, where L_{AB} and L_{BQC} are self-inductance of the straight filaments and the folded filaments, respectively; M_{AB-CD} and $M_{BQC-APD}$ are the mutual inductance between the two straight filaments and the two folded ones. The values of self-inductance and mutual inductance can be calculated by theoretical equations[33] (see Note S1 for detailed calculation, Supporting Information). As shown in Figure 1B, the self-inductance of the straight filaments is constant, while self-inductance of the folded filaments (L_{BQC}) decreases with the folding angle. Mutual inductance between the two straight filaments (M_{AB-CD}) increases significantly as folding brings the two straight filaments closer (stronger magnetic field coupling), making the major contribution to the decrease of the total inductance. However, mutual inductance between the two folded filaments decreases with the folding angle, which would increase the total inductance. When a rectangular coil is folded along its long axis (AB > BC), then $L_{AB} > L_{BC}$, $M_{AB-CD} > M_{BC-AD}$, which makes the total inductance variation higher. In summary, the higher the aspect ratio (AB/BC) of a rectangular coil, the higher the inductance variations caused by a specific folding angle (Figure S1C, Supporting Information). However, it should be noted that, theoretically, any rectangular coil (no matter the aspect ratio) would reach a null total inductance when it is fully folded ($\beta = 180°$) since the magnetic field generated by the two halves of the coil would completely cancel each other. In practice, most planar coils are made of more than 1 turn (e.g., 10 turns for the rectangular coil shown in Figure 1A), and the coil shape could be circular, rectangular, or more complex (e.g., hexagonal). In any of these cases, it is difficult to perform theoretical analysis.

2.1.2. Finite Element Analysis

Finite element (FE) analysis has been widely used to simulate the electromagnetic phenomena, including 2D and 3D coils.[19b] Given that the dimension of the coil trace (≈0.1 mm) is at least 2 orders of magnitude smaller than the overall size of the coil (≈10 mm), a significant number of elements would be needed in a 3D FE model, easily overwhelming the computational capabilities of the used system. In addition, creating the CAD model of the folded or bent coil traces could be challenging as well.

Since the inductance is proportional to the magnetic field energy a coil stored when one unit of electric current flowing through it, the change of magnetic field density (B) and distribution due to bending or folding can provide some insights for the inductance variation. A simplified 2D FE model was created in COMSOL Multiphysics (see more details in Note S2, Supporting Information), to investigate the magnetic field distribution of the cross-section of a long rectangular coil (where the length is much greater than the width, and contributions from traces along the width and near the corners are negligible). The cross-section of a 10-turns rectangular coil surrounded by air was created for the FE model (Figure S2, Supporting Information), and its MF distribution was calculated (Figure 1C-I; and Figure S2A, Supporting Information). Then, the coil traces were folded into two halves at different angles, the magnetic flux lines show that the magnetic fields generated by the two halves of the coils increasingly repeal each other with the increase of the folding angle (Movie S1, Supporting Information). The magnetic field energy is highly concentrated at the region enveloped by the two halves of the coil (areas with bright color, higher B), particularly when the folding angle is large (150° for Figure 1C-II). Figure 1C-III shows the magnetic flux and density of the planar coil bent by 300°, which indicates similar changes of magnetic field distribution with respect to the folded coil, although these changes are smaller (Figure S2 and Movie S1, Supporting Information).

It has been reported that the fabrication of high-value inductors can be realized by folding single-layer multicoils into a stacked multilayer coil.[34] To further investigate the total inductance change during folding of a planar dual-coil, namely two planar coils placed next to each other on the same plane, FE modeling of dual-coils with the same/opposite current flow directions were also performed. As shown in Figure S2C,D (Supporting Information), the magnetic fields generated by the two coils superpose onto (cancel) each other when their current flows are the opposite (the same), thereby the increase (decrease) of the total inductance. Considering the magnetic field energy, when two layers of planar coils stack together with the same current flow directions, the total inductance is almost four times of single-coil, while if the current flow is opposite, the total inductance would be close to zero.

2.1.3. Numerical Analysis

Since neither the theoretical analysis nor the FE modeling can effectively provide a quantitative analysis of the inductance change due to folding and bending of planar coils for complex geometries and multicoils, we developed our own tools to address this issue through numerical analysis (see Note S3 for more details, Supporting Information). From the literature, self-inductance of 2D (planar coils) or 3D (folded/bent coils) wire loop can be calculated as a curve integral[35] akin to the Neumann formula. When the wire loop is discretized into hundreds to thousands of small segments (Figure S3, Supporting Information), the numerical integration can be performed efficiently in many computational programming languages (e.g., MATLAB).

Folding and bending can be achieved by applying simple coordinate transformations on the cross-section of the planar coils, as detailed in Figure 1D,E. For a rectangular planar coil (depicted in Figure 1A) folded by 45°, 90°, and 135°, Figure 1D shows the inductance decrease to 95.9%, 82.8%, and 56.4% of its original inductance ($L_0 = 3.6303$ µH), respectively. Unlike in studies on bending curvature measurement, here the bending angle β, instead of curvature/radius, is used to define the degree of bending given that the bending angle is dimensionless (regardless of the coil size). Then, the bending radius R (curvature $K = 1/R$) of the planar coil can be calculated when it is needed by $R = s/\beta$, where s is the length of the arc, which equals the width of the planar coil. Figure 1E shows the shapes of the rectangular coil bent by 90°, 180° (semicylinder), and 270°, resulting in a decrease of inductance to 97.7%, 90.5%, and 77.3% of L_0, respectively. This result confirms the qualitative results from the FE modeling that bending of a planar coil

**ADVANCED
SCIENCE NEWS**
www.advancedsciencenews.com

**ADVANCED
MATERIALS
TECHNOLOGIES**
www.advmattechnol.de

causes less magnetic field change than folding, thereby smaller inductance decrease.

In a real-world scenario, planar coils cannot be folded along an axis on the coil plane with zero radii given that the coil traces and substrate have a definite thickness and minimal bending radius. Thus, a planar coil cannot be folded by 180° with its two halves completely overlapped in space, no matter how thin the planar coil is. Therefore, for a physical device, a small arc near the folding axis always occurs when a thin planar coil is folded. The arc length s can be defined by the minimum bending radius of the planar coil film: $s = \pi R_{min}$ (Figure 1F). Hence, in a real-world case, planar coil folding is a combination of bending of a small arc part near the folding axis and folding of the rest of the coil. Figure 1F shows the shapes of the rectangular coil folded by 45°, 90°, and 135° with an arc length of 6.28 mm (R_{min} = 2 mm), its inductance decreases to 97.3%, 88.8%, and 73.1%, respectively. Animations of shape transformations and inductance variations of planar coils (both rectangular and circular coils) caused by folding, bending, and folding with an arc are presented in Movie S2 (Supporting Information).

The results described above highlight that folding with a small arc is an intermediate case between ideal folding and pure bending, which causes an inductance decrease less than folding without arc (ideal folding), but higher than the case of pure bending. Furthermore, it can be expected that the shorter the folding arc is, the larger the inductance changes. Figure 1G shows curves of normalized inductance against folding angle with different folding arc lengths (s = 0, 1, 2, 5, 10, and 25 mm). When the folding arc length equals the width of the planar coil (s = 25 mm), it transits to the case of pure bending. Experimental results of folding (diamond marker) and bending (circle marker) of an FPC coil is also plotted in Figure 1G for comparison. The experimental results of the flexible coil folding approximate well the numerical analysis results of the case of folding with a 2 mm arc (R_{min} = 0.64 mm).

2.2. Coil Design Parameters

In this work, we utilized two types of planar coils for folding and bending characterization, cyclic testing, sensing performance evaluation, and case studies. One type is the FPC coil made of copper traces on polyimide substrate, while the other type is the LM coil made by direct printing of liquid metal-based ink on polydimethylsiloxane (PDMS) substrates (see the Experimental Section for more details). Throughout this manuscript, each coil is labeled with its dimension (length and width for rectangular coils, diameter for circular coils) followed by the pitch of its wire loops, for instance, "L50W25P1.0" refers to a rectangular coil with a length of 50 mm, width of 25 mm, and 1.0 mm pitch. Parameters of all FPC and LM coils are listed in Table S1 (Supporting Information).

First, LM and FPC coils with the same design (L50W25P1.0) were tested for folding and compared with numerical analysis results (Figure S5B, Supporting Information). The results show that the two types of coils have almost exactly the same inductance change to folding angle, despite they are made of different conductive and substrate materials, with different resistances (14.43 and 124.6 Ω for the FPC and LM coils, respectively). This

is also in good agreement with the numerical analysis results of folding with a 2.2 mm arc, with a maximum difference of only 1.3%. It should be noted that the FPC coils are not literally soft, due to the double layer copper traces (35 µm thick) and multiple layer of polymide films. In this study, they were used as experimental platform since the fabrication are rather mature, and reliable, to guarantee a consistent quality with various coil design. Given that this sensing approach is insensitive to the coil and substrate materials, any other fabrication technology can be explored to make thin, soft planar coils that meet the requirements of a specific application with the same characteristics.

To investigate how the coil design affects its inductance variation to folding and bending, FPC coils with different shapes, pitches, and sizes (Figure S4, Supporting Information) were characterized. Theoretical analysis results already provided some insight on how the aspect ratio of rectangular coils can affect the inductance change due to folding. Here, rectangular coils with different aspect ratios and circular coils were investigated through experiments and numerical analysis. As shown in **Figure 2**B, the shorter coil (rect-1:2) is less sensitive to folding than the longer ones (rect-1:1 and rect-2:1), whereas the circular coil shows the highest sensitivity as the inductance decreases to 57.6% at 150° (also confirmed by numerical analysis in Figure S6A, Supporting Information). However, for rectangular coils with a length greater than its width, the differences are only 0.2% at 150°. As shown in Figure 2C, the coil shape has a much more significant effect for the pure bending case as inductance to bending angle curves of the four coils differs from each other. Similarly, a long rectangular coil has a much higher inductance variation compared to short rectangular coils. The difference is that, the circular coil has a rather small inductance variation, just slightly larger than the short rectangular coil (rect-1:2). Numerical analysis results show the same coil shape effect (Figure S6B, Supporting Information). We also characterized the case of dual-coils with opposite and same current flow directions, to verify our assumptions from FE modeling and to compare the results with single-coil. The total inductance of the dual coil with opposite direction increases to 121.7% at 150° folding, while the inductance decreases to 73.52% for dual-coil in the same direction, in comparison with 58.76% for the single-coil. Although it seems that the dual-coil is less sensitive than single coils, dual-coil with opposite direction could be still a good design option given that its inductance increases with folding angle.

The theoretical analysis suggests that the mutual inductance of the unfolded filaments of the coil makes the biggest contribution to the total inductance decrease. Therefore, it can be predicted that a larger pitch in the width direction (PW) might increase the inductance change, as more traces are closer to the folding axis (higher mutual inductance). To validate this assumption, square FPC coils (rect-1:1) with different pitches in the length and width directions were characterized. Both experimental (Figure 2E) and numerical (Figure S6D, Supporting Information) results confirm that coils with larger PW (0.8 mm) have a higher inductance decrease to 46.48% at 150° (55.61% for the coil with PW = 0.3 mm and PL = 0.3 mm), while PL does not affect much. Results for circular coils also show that the larger the pitch, the higher the inductance
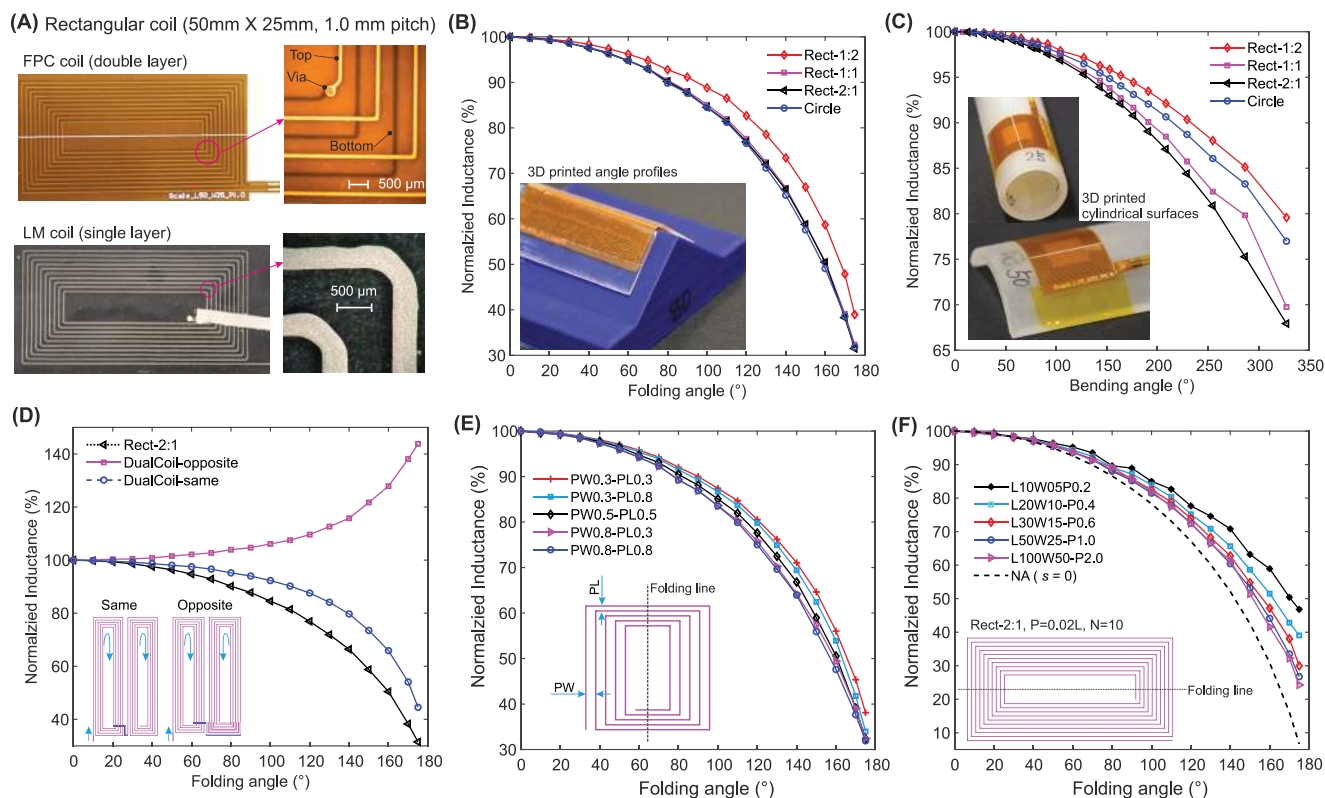
ADVANCED
SCIENCE NEWS
www.advancedsciencenews.com

ADVANCED
MATERIALS
TECHNOLOGIES
www.advmattechnol.de

Figure 2. Static characteristics of folding and bending of planar coils with different design parameters (shape, pitch, size). A) Images and magnified images of a FPC coil and a LM coil. B) Inductance variation to folding angles of planar coils with a different shape (circle, square, rectangle 1:2, rectangle 2:1). C) Inductance variations against bending angle of planar coils with different shapes. D) Inductance variation against folding angle of dual-coils compared with a single coil with the same overall dimension. E) Inductance variations of square coils with different pitches in width and length directions. F) Inductance variations of rectangular coils (2:1) with different size (from 10 to 100 mm).

change (Figure S6E, Supporting Information). In summary, a long rectangular coil with large pitches in the width direction would result in higher inductance change to folding, as well as circular coils with a large pitch (small inner diameter).

Given that the inductance of a coil is determined by the geometry of its conductive traces, a coil's inductance is proportional to its size. For coils with the same design, the normalized inductance to folding angle should be the same when the coil is scaled up or down. Rectangular coils (having a length to width ratio of 2, and pitch is 2% of its length) with 10 turns were used to evaluate the scalability of this mechanism. In the numerical analysis results of folding without arc, the responses for such coils with different sizes are exactly the same (Figure S6F, Supporting Information). Instead, experimental results show that smaller coils have a relatively smaller inductance change, with inductance down to 63.2% and 51.4% at 150° for coil L10W5 and coil L100W50 respectively, since the folding arc affects smaller coils more significantly. This effect is confirmed by numerical analysis of folding with a fixed arc length of 1.6 mm for coils at all sizes, where smaller coils have a lower inductance change (Figure S6F, Supporting Information). Nonetheless, these results highlight that this sensing mechanism is scalable that folding sensors made of the same coil design have very similar responses across one order of scale (e.g., 10–100 mm) or even more, facilitating adoption of this sensing mechanism

in different scenarios. By reducing the conductive traces/gaps to 10 µm range with microfabrication technologies, the planar coils can be miniaturized. Although, in practical applications, it is sensible to believe that 2–3 mm is the minimum coil diameter or length/width allowing a sufficient quality factor ($Q = 2\pi f L/R$), in order to achieve good signal to noise ratio in the sensing system.

2.3. Cyclic Folding and Bending

To evaluate the dynamic characteristics of planar coils, bending and releasing (0°–180°) cycles were applied to a rectangular FPC coil (L50W25P1.0) by moving one side of the coil close to the other, employing a motorized linear stage (**Figure 3**A; and Movie S3, Supporting Information). Both side edges of the flexible coil were connected to rigid acrylic plates with flexure hinges (see more details in the Experimental Section). Results show that the FPC coil's inductance decreases to 91.2% when bent to a semicylindrical surface (180° bending angle), and inductance to distance curves during the bending and releasing phases are almost completely overlapped (Figure 3B), with negligible hysteresis (<1.0%). Cyclic tests also suggest that the inductance response is highly stable and repeatable even after 1000 cycles of bending-releasing (Figure S7, Supporting Information).
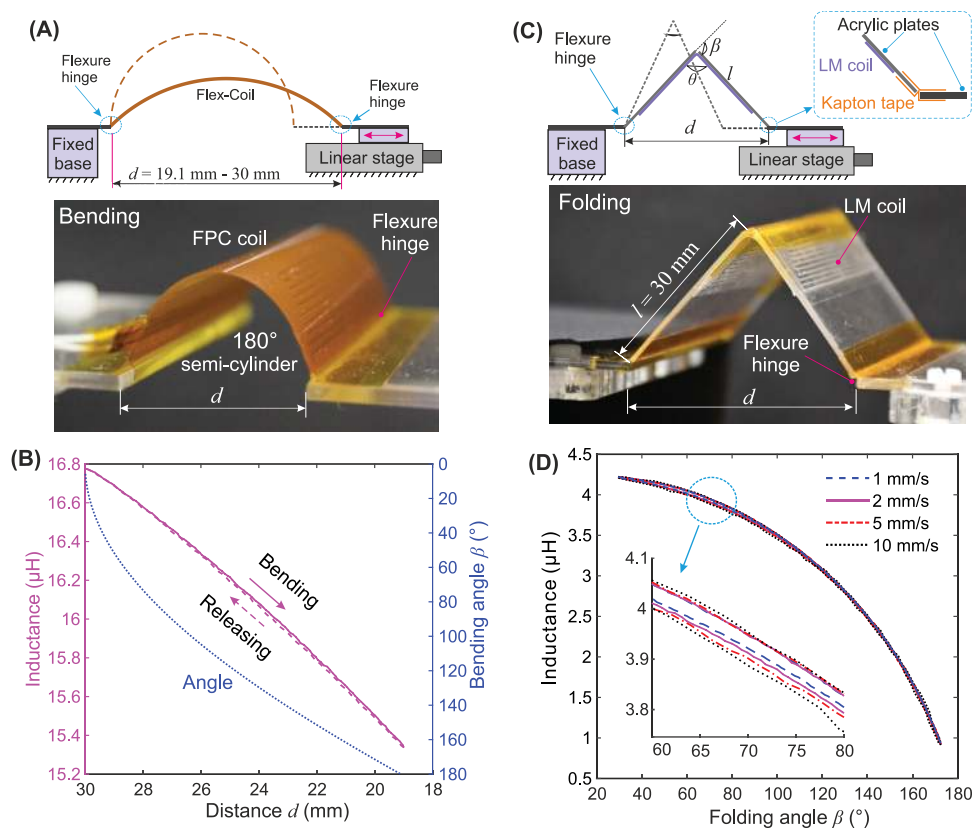
**ADVANCED
SCIENCE NEWS**
www.advancedsciencenews.com

**ADVANCED
MATERIALS
TECHNOLOGIES**
www.advmattechnol.de

Figure 3. Cyclic bending and folding test. A) Experimental setup for dynamic coil bending test. B) Inductance variations of a FPC coil bent to 180° (semicylinder). C) Experimental setup for dynamic coil folding test. D) Inductance variation of a LM coil folded-unfolded at different velocities (1, 2, 5, and 10 mm s^{-1}).

As shown in Figure 3C, a rectangular LM coil (L50W25P1.0) was fixed on two acrylic plates to form the flexure hinge as the folding axis, then two sides of the acrylic plates were connected to the fixed base and linear stage with flexure hinges, respectively (see the Experimental Section for more details). Cyclic folding tests of the LM coil were performed at different velocities of the linear stage, from 1 to 10 mm s^{-1}. As shown in Figure 3D, the curves of the first folding–unfolding cycle (30°–150°) for all velocities are almost overlapped, with negligible hysteresis (only 0.92% at 1 mm s^{-1}). From the magnified curves (inset of Figure 3D), it can be noticed that hysteresis at higher speed is slightly larger (2.0% at 10 mm s^{-1}), which is most likely caused by the backlash and acceleration/deceleration phase of the linear stage's movement. In summary, unlike most strain-based angle sensing system, the SIAS is velocity-independent and hysteresis-free, which is a crucial feature for soft sensors to guarantee accurate measurement of all types of angle change (no matter the magnitude or speed). In the case of cyclic folding/unfolding test of FPC coils, we observed some delamination near the folding axis of the FPC coils after hundreds of cycles (Figure S8C and Movie S4, Supporting Information), eventually, the copper trace of the FPC coil broke due to common metal fatigue indicated by the drastically increased resistance (Figure S8E, Supporting Information). Therefore, the folding arc length (minimal radius) should be larger to extend the FPC coil's lifetime in folding sensing

applications. From this point of view, the dual-coil configuration presented in Figure 2D would have advantages. For applications that require thousands of folding and unfolding cycles, planar coils made of thin, soft, and durable materials (e.g., LM coils, printed coil on thin polymer films) should be used. In this case, the planar coils are compliant enough (extremely low bending stiffness) to passively follow the deformation/movement of the hosting body without introducing any constraint.

2.4. Sensing Performance

To demonstrate the high sensitivity and accurate response of the SIAS, step angle changes were applied to the test platform (Movie S4, Supporting Information). Inductance variations due to 1° and 0.1° incremental angle changes were plotted in **Figure 4**A,B, respectively, with reference angles (blue dashed line) calculated from the real-time position of the linear stage. The folding sensor has a sensitivity of 39.25 nH/° when the angle between two halves of the LM coil is around 30° ($\beta = 150°$). It this case, the inductance measurement noise is only 0.034 nH (root mean square (RMS)) based on 60 s data collected from the inductance-capacitance-resistance (LCR) meter with 5 Hz sampling rate. Thus, the minimal detectable angle variation (resolution) is as low as 0.000 87° (15 μrad). It is worth to mention that the inductance measurement noise for FPC
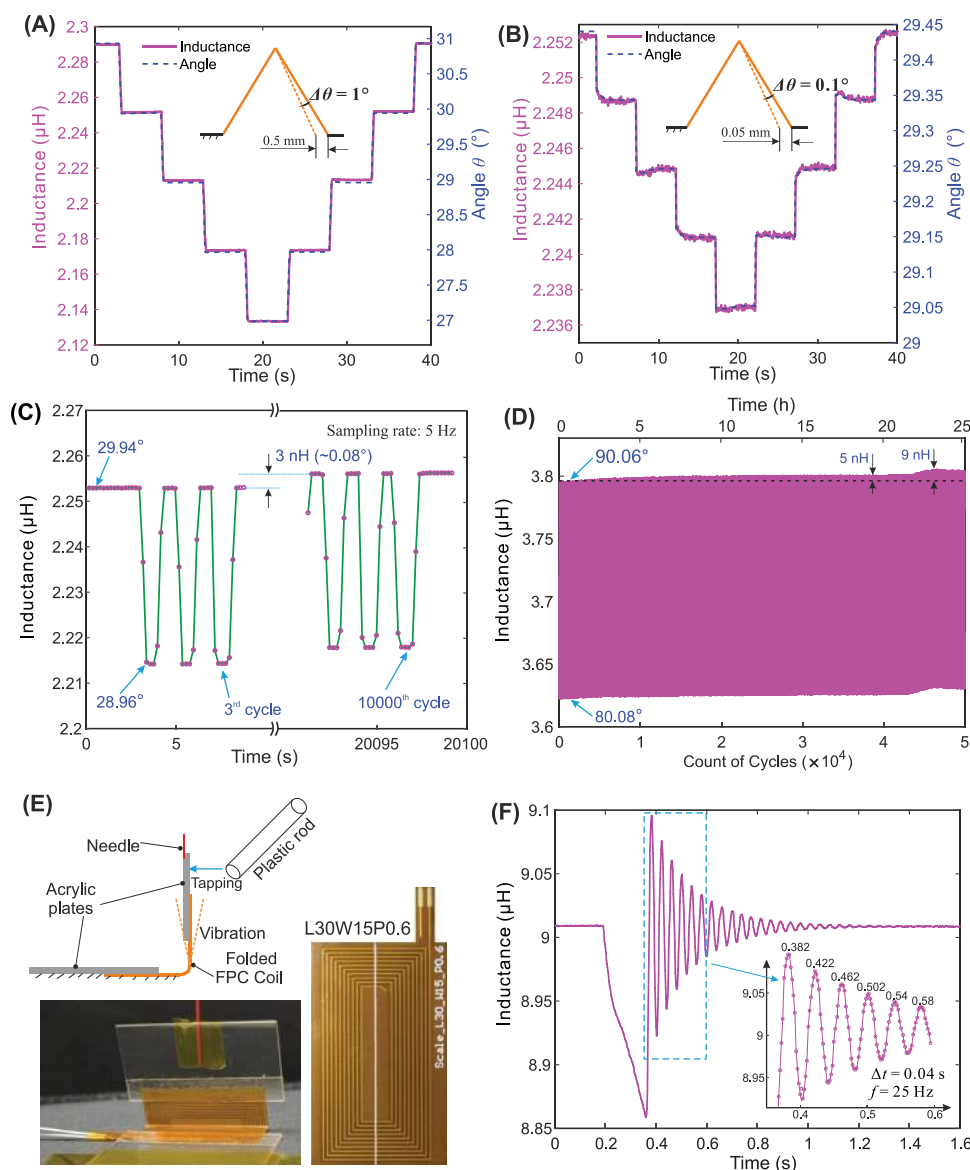
Figure 4. Folding angle sensing performance evaluation. Inductance variations of folding angle changes of A) 1° step; B) 0.1° step; C) Inductance variation of 1° folding angle changes (switch between 29° and 30° with 1 s stop at each angle) for 10 000 cycles. D) Results of 50 000 cycles continuous folding–unfolding test with an angle variation of 10° (80°– 90°). E) Sketch of a cantilever beam structure made of a folded FPC coil and two acrylic plates, images of the device and the FPC coil used (L30W15P0.6). F) Inductance variations of the prefolded FPC coil when the cantilever beam tapped by a plastic rod which introduces vibrations.

coil at the same condition is even lower (0.020 nH, RMS) given that it has higher inductance value but much lower resistance (i.e., higher quality factor).

Furthermore, a test of 10 000 cycles of 1° angle change was performed to highlight the extremely high sensitivity and stability of this type of angle sensing approach. As shown in Figure 4C, during the 5 h and 25 min cyclic test, the inductance variations caused by the 1° angle change remains exactly the same (Figure S8D, Supporting Information), and the maximum fluctuation of the absolute inductance value is only 3 nH (equals 0.08° angle measurement error). During the same time, the series resistance shows a continuous, unpredictable increase caused by ambient temperature and/or other factors

(Figure S8D, Supporting Information). In addition, another 50 000 cycles continuous folding and unfolding test of the same LM coil with an angle variation of 10° (80°–90°) was also conducted. The result (Figure 4D) indicates that the absolute inductance value has a very small drift of 5 nH for the first 40 000 cycles, and a maximum drift of 9 nH (equals 0.51° angle error) during the whole experiment period (25.1 h). The excellent long-term stability of this type of sensor benefits from the fact that the sensing response is insensitive to electrical and mechanical properties of the conductive coil traces and substrate materials.

Most soft sensors, particularly strain-measurement sensors show very poor performance for dynamic measurement due to their slow response and large hysteresis. On the contrary, the

**ADVANCED
SCIENCE NEWS**
www.advancedsciencenews.com

**ADVANCED
MATERIALS
TECHNOLOGIES**
www.advmattechnol.de

SIAS can achieve rapid response to dynamic angle changes as well as static ones (see the Experimental Section for detail of the fast inductance measurement). As shown in Figure 4E, a simple cantilever structure was built to test the sensor's dynamic response, consisting of a folded FPC coil with two acrylic plates attached. The upper half of the coil-acrylic plate acts as a cantilever plate, which would produce vibrations when an impact load is applied (e.g., tapping). The results show that the sensor can clearly record the oscillation wave of the angle changes due to vibration (Figure 4F; and Movie S5, Supporting Information). The curve of the inductance value indicates that the vibration amplitude decays to zero in about 1 s due to the damping effect, and the resonance frequency of this cantilever structure is about 25 Hz. This test demonstrated that the sensor has an excellent dynamic response, which can provide rich information like impact and contact detection, even inherit mechanical properties (e.g.,: self-resonance frequency) of the system itself.
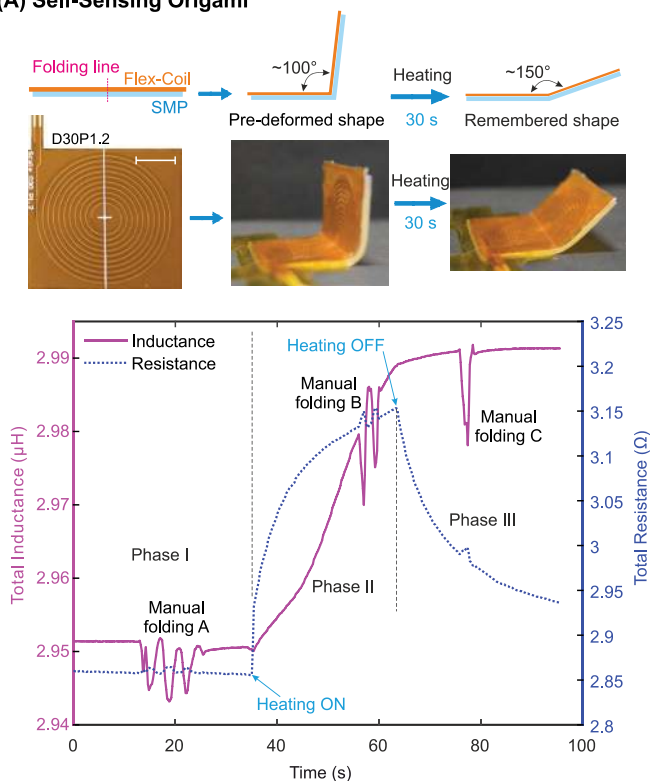
2.5. Case Studies

In order to highlight the advantages and versatility of the SIAS, planar coils were deployed for simultaneous angle sensing and thermal actuation in a self-sensing origami structure, bending curvature/angle sensing of a soft pneumatic actuator, and wearable sensing of elbow angle.

2.5.1. Self-Sensing Origami

The majority of origami robots are based on/off open-loop control, and rely on predefined folding sequences to perform programmed tasks. Shape memory polymers (SMP)[36] are one of the smart materials previously exploited for developing artificial muscles and origami robots. Here, we present a simple bilayer origami structure (open-up under heating) made of a layer of SMP sheet bonded together with a FPC coil (D30P1.2). In this bilayer structure, the FPC coil can achieve both actuation (through Joule heating) and self-sensing of the folding angle (through inductance measurement) simultaneously. As shown in **Figure 5**A, the bilayer origami structure was predeformed at around 100°, and it opened up to the remembered shape with an angle around 150° after being heated for 30 s. By measuring the inductance, not only the angle variation of the origami structure caused by thermal actuation can be monitored, but also the angle variation introduced by external stimuli (manual folding A, B, and C) at any of the three phases are detected (Movie S6, Supporting Information). For case B of manual folding, the inductance records the total angle change caused by the internal-driven slow unfolding and the external manual-folding and unfolding. The results for this simple bilayer structure are encouraging and hold promise for building simultaneously sensing and actuation in origami robots, enabling closed-loop control and intelligent interaction with the environment.
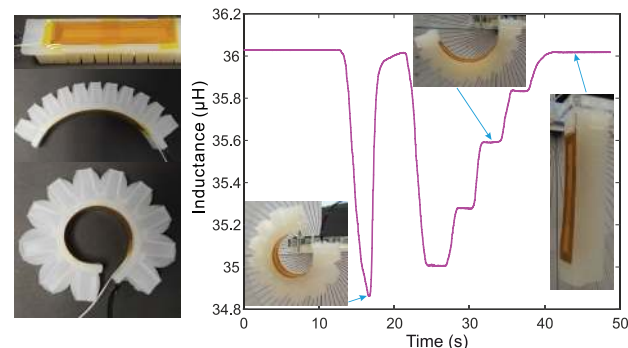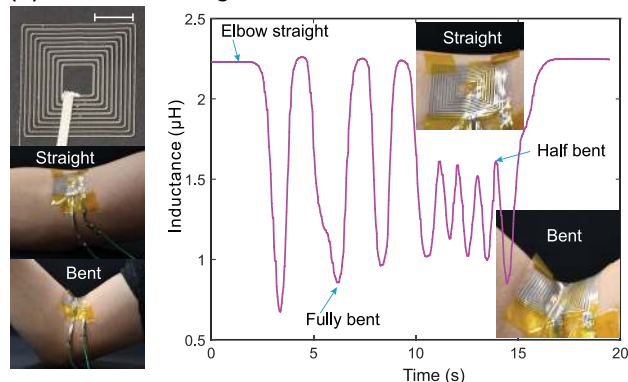

Figure 5. Case studies of planar coils for angle sensing in different scenarios. A) A circular FPC coil for simultaneous actuation (heating the shape memory polymer film) and sensing of the angle change caused by the actuation and/or external stimuli (scale bar: 10 mm). B) A rectangular FPC coil to sense the bending angle/curvature of a classic PneuNet type bending actuator. C) A square LM coil was attached to the inner side of the elbow to monitor the angle (scale bar: 10 mm).

**ADVANCED
SCIENCE NEWS**
www.advancedsciencenews.com

**ADVANCED
MATERIALS
TECHNOLOGIES**
www.advmattechnol.de

Moreover, the resistance curve gives clear indications of the time when the heating is switched on/off. And temperature information of the structure can be obtained from the coil resistance since the resistivity of the copper trace increases with temperature (0.004 °C). Figure 5A shows that the resistance increases rapidly after the heating is switched-on (phase II), then gradually decreased after the heating is turned-off (phase III). It should be noted that the inductance and resistance measured and plotted in Figure 5A is the total inductance and total resistance of a network (including the FPC coil, a DC isolation capacitor, and the impedance of the DC power supply, Figure S9A, Supporting Information), instead of the coil itself. Details of the electronic circuit and impedance relationship can be found in Note S4 (Supporting Information).

2.5.2. Sensorized Soft Pneumatic Actuator

In this case, a long rectangular coil (L75W16P0.5) was attached to a classic PneuNet type bending soft pneumatic actuator (SPA)[37] to demonstrate the easy-to-implement feature of the SIAS for bending curvature/angle sensing (Figure 5B). For this type of bending SPA, the inner side surface is very close to the neutral bending plane, which would make it difficult for common strain type sensors to detect the bending curvature if the sensor is attached to this surface. The outer surface of this SPA has much higher tensile strain when it is bent but obviously not suitable to host the strain sensor given its structure. Benefiting from the fact the SIAS operates through magnetic field coupling in space, the FPC coil can detect the bending curvature/angle of a surface where it is attached to. In this case, the FPC coil bends with the SPA, so the bending curvature/radius of the FPC is the same as the SPA. As shown in Figure 5B, the inductance of the FPC coil precisely recorded that the SPA was fully actuated to roll into ring-shape, then actuated with incrementally lower pressures (Movie S7, Supporting Information). In a more complex soft robotic system, the proprioception capability could be addressed in the future by embedding multiple planar coils during the fabrication of the soft body or simply sticking the printed coils on targeted surfaces.

2.5.3. Wearable Sensing

Remarkable achievements have been made in wearable systems in the last decade, by utilizing technologies like textile-based garments[8] and skin electronics,[38] for applications spanning from activities monitoring (body gesture, respiration, movement, vocalization, etc.), healthcare devices, to augmented reality. The majority of these monitoring systems are based on a strain-sensing approach, which requires good stretchability and adhesion of the sensing film on human skin to provide a reliable measurement. In contrast, as a nonstrain-measurement, directly angle sensing approach, planar coils can measure the angle of a curved surface by simply sticking on it. As shown in Figure 5C, a square LM coil (L30W30P1.2) was attached on the inner side of a person's elbow by Kapton tape. When the arm moves from a straight to a full bent state, or from full bent to half-bent states, the inductance value clearly indicates

the angle of the elbow (Movie S8, Supporting Information). It can be noticed that the LM coil was not attached firmly on the skin, and some wrinkles appeared when the elbow was bent, but angle measurement is not affected. As discussed in the introduction, this type of angle sensing approach can achieve much better performance (reliability, accuracy, and robustness) in wearable sensing, particularly when unknown local deformation presents. For example, if the coil is folded/bent with a bit twisting (i.e., one side of the coil is folded/bent with a larger angle than the other side), the sensor would still give accurate measurement by providing an average value of the folding/bending angle since the coil's inductance is determined by the overall 3D geometry (magnetic field coupling in 3D space). In the future, planar coils can be also utilized in a wearable skin electronic systems for both angle sensing and wireless communication/powering.

3. Conclusion

In summary, we present the SIAS, a new mechanism that transforms planar coils into film-like, highly-precise, scalable, versatile folding, and bending angle sensors. A numerical analysis tool was developed to efficiently calculate the inductance change of planar coils due to folding, bending, and folding with a small arc (the real case for physical devices), which would be also useful to investigate the characteristics of planar coils undergo complex deformations (e.g., in flexible and stretchable electronic systems). Unlike the strain-based angle sensing approaches, the SIAS is velocity-independent and hysteresis-free, ensuing accurate measurement in real-world applications no matter the angle change is small or big, fast, or slow. Experimental results also indicate that the SIAS is extremely stable and ultrasensitive (high resolution).

It should be acknowledged that the SIAS must be implemented in systems made of nonconductive, nonferromagnetic materials only, since a coil's inductance can be reduced or enhanced by conductive or ferromagnetic objects nearby (previously adopted for pressure sensing). Utilizing more than one of these inductive transduction principles, planar coils could be further exploited to develop multimodal sensors to sense bending/folding angle, as well as pressure, paving the way for developing soft perceptive robots for example. Ideally, planar coils made of thin, complaint (extremely low bending stiffness) materials are the best option for bending curvature sensing, as the coils can passively follow the deformation/movement of the hosting body without introducing any constraint. The plane coil films (with limited stretchability) should be implemented on the neutral plane of the soft bending body or the compressed side since this type of sensor does not rely on strain measurement. When stretchable coils (e.g., LM coil) are used, stretching of the coil should be avoided as the coil's inductance would be increased when stretched, canceling part of the inductance decrease caused by bending. In this view, we are investigating a solution to distinguish the bending and stretching for stretchable coils. In the case of complex deformation with different bending curvatures/directions along the length, multiple coils would be needed to obtain the local curvatures. For example, a row of planar coils can be printed on a flexible ribbon to

**ADVANCED
SCIENCE NEWS**
www.advancedsciencenews.com

**ADVANCED
MATERIALS
TECHNOLOGIES**
www.advmattechnol.de

reconstruct the shape (proprioception). In this case, both the self-inductance of individual coil and mutual inductance between coils next each other can be utilized to provide sensing information.

Furthermore, since the SIAS operates through magnetic field coupling in space, it is independent from electrical and mechanical properties of the conductive traces and substrate materials, and insensitive to local defects in fabrication or integration. Moreover, it is scalable and can achieve fast response as it is only limited by the bandwidth of the electronics needed for the inductance measurement (as demonstrated for vibration detection). It should be noted that the coil can be easily scaled up, whereas it is rather difficult to scale down compared to capacitive sensors. Given that a planar coil's inductance is proportional to its dimension, 2–3 mm would be the minimum size in practical applications to achieve good signal to noise ratio. The self-inductance of a planar coil at a size smaller than 2 mm (0.1–1 µH) would be comparable to the inductance of short leading wires, resulting in poor robustness of the measurement. Stacking more layers of planar coils can significantly increase the inductance (square growth), but at the cost of increasing the thickness of the sensor (bending stiffness) and the fabrication complexity.

Besides these unique advantages in angle sensing performance, the SIAS can be easily fabricated through various available technologies at low-cost, and it is extremely easy to implement in application systems by simply sticking a planar coil film on the targeted surface, or even directly printing the coil traces on it. Moreover, planar coils can be employed as multifunctional components for both inductive sensing and wireless communication/powering, facilitating simple system design. All these desirable features and potentials make the SIAS promising for applications in robotics, wearable systems, and beyond.

4. Experimental Section

Design and Fabrication of FPC Coils: Patterns of each planar coil were created in AutoCAD based on its specific parameters (shape, dimension, pitch), then imported into Altium designer to form the layer out of the conductive trace. As depicted in Figure S4B (Supporting Information), all FPC single coils have double layers with 10 turns on each layer, with one layer in clockwise, while the other is counter-clockwise, connected through vias in their middle terminals. FPC dual-coils and LM coils have only one layer with 10 turns. Design parameters, inductance and resistance values of all coils are listed in Table S1 (Supporting Information). All FPC coils (Figure S4, Supporting Information) were manufactured by a PCB manufacturer (Linghangda Technology Co., Ltd, Shenzhen, China) in one batch. Cross-section structure of the FPC coils are illustrated in Figure S4C, Supporting Information, with a thickness of the copper traces of 35 µm, a width of 100 µm, and various spaces between traces according to the pitch of each coil. Dielectric (65 µm) and insulating (50 µm) layers are made of polyimide (PI, also called Kapton) films. The total thickness of the FPC coil is 235(±30) µm.

Fabrication of LM Coils: LM coils (Figure 2A) were directly printed by dispensing liquid metal micro-particles (LMMP) ink on PDMS substrate with a nozzle printer (nozzle diameter: 100 µm, velocity: 3 mm s^{-1}, Musashi, Image Master 350PC, Japan), then annealed at 100 °C for 3 h to remove the solvent. The LMMP suspension was prepared by high power ultrasonication of bulk EGaIn, following the

reported procedure.[39] A weak ultrasonication was applied before nozzle printing. The LM trace has a width of 300 µm, and a thickness of 20 µm. Another thin layer of PDMS was printed on top to completely encapsulate it. The total thickness of the LM coils is approximately 500 µm. Conductive textile strips (4712, Holland Shielding Systems BV, the Netherlands) were attached on both terminals of the LM trace to achieve good mechanical and electrical connection for inductance and resistance measurement.

Static Characterization of Planar Coil Folding and Bending: Triangular convex surfaces with angles from 0° to 170° with 10° increment (plus 175°) were 3D printed as profiles for folding characterization (Figure S5A, Supporting Information). Each FPC coil to be tested was pre-folded along the central line and attached to two acrylic plates (0.8 mm thick) to ensure it is evenly folded across the folding axis. Then, the two acrylic plates on the FPC coil were pressed against the two side walls of an angle profile to ensure the right folding angle, and the inductance value of the coil was recorded through an LCR meter (Agilent E4980A, Keysight Technologies, USA) at 200 kHz. LM coils were prepared and tested with the same procedure. Cylindrical tubes, rods, and surfaces with the designed diameter (curvature) were 3D printed for pure bending testing (Figure S5D, Supporting Information). FPC coils were rolled firmly on the cylindrical surface with two sides fixed by Kapton tape, then the inductance value was recorded.

Experimental Setup for Dynamic Testing: Dynamic testing of the FPC coil bending was achieved by using a motorized linear stage (M-414.1PD, Physik Instrument, Germany) to compress the two sides of an FPC coil and to bend it to certain angle/curvature (Figure S7, Supporting Information). Two sides of the FPC coil were connected to rigid acrylic plates (1.5 mm) with thin Kapton tape (20 µm) to form flexure hinges to allow free rotation between the coil and the acrylic plates. The distance between the two sides of the curved coil was controlled by moving the linear stage to the targeted position, subsequently, the inductance was recorded with the corresponding curvature (bending angle). The coil was bent to a maximum angle of 180° (a semicylinder surface), ensuring constant curvature across the bending arc. A customized program (LabView, National Instruments, USA) was developed to control the movement of linear stage and to record inductance value from a LCR meter. Similarly, the FPC and LM coils were attached to thin acrylic plates (0.8 mm) like in the static testing, and two sides of the thin acrylic plates were connected to thick acrylic plates (1.5 mm) through flexure hinges made of Kapton tape. Thus, the linear movement of one side of the acrylic plate was translated into the angle change (folding and unfolding) of the planar coil (Figure S8, Supporting Information).

Preparation of the Self-Sensing Origami: A 0.8 mm thick square SMP sheet (Durable resin, FLDUCL02, Formlabs, USA) was cast in a 3D printed mold and cured under UV light. An FPC coil (D30P1.2) was pre-folded, then unfolded, and glued on the flat SMP sheet with Epoxy adhesive. After applying 0.8 A current through the FPC coil to heat the SMP and soften it, the bilayer structure was predeformed around 100° and slowly cooled down to room temperature while maintaining the shape. In the demonstration (Figure 5A), 0.8 A DC current was applied to the FPC coil for about 30 s to produce the heat to drive the structure to unfold to 150°.

Fabrication of the Soft Pneumatic Actuator: Fabrication of the bending soft pneumatic actuator followed the procedure of the "PneuNets Bending Actuators" provided by Polygerinos et. al. in the soft robotic toolkit.[40] CAD files were downloaded and 3D printed (Ultimaker S3, The Netherlands) with tough PLA. Dragon-Skin 10 (Smooth-On, USA) was used to cast the elastomeric body of the SPA by following the exact steps.

Inductance Measurement: All the inductance values were measured by a precision LCR meter (Agilent E4980A, Keysight Technologies, USA) at 200 Hz, except in the case of vibration detection, which requires a much higher sampling rate. An LC oscillator-based approach (Figure S9B, Supporting Information) was deployed to measure the inductance value with high speed and high resolution. A fully integrated inductance to digital converter chip (LDC1614, Texas Instruments, USA) was used to

**ADVANCED
SCIENCE NEWS**
www.advancedsciencenews.com

**ADVANCED
MATERIALS
TECHNOLOGIES**
www.advmattechnol.de

form the LC oscillator, measure the frequency, convert into digital data, and subsequently sent to a microcontroller (NI myRIO 1900, National Instruments, USA) via I2C protocol. A 100 pF NP0 capacitor was used in the LC network, while the inductance value is ≈9 µH when the FPC coil is folded at 90°, which gives an oscillation frequency of 5.3 MHz. The sampling rate in the demonstration was set as 500 Hz (about 20 points per vibration cycle) to achieve a balanced speed and resolution However it can be increased up to 4 kHz if needed, at the cost of a lower resolution (higher noise).

Study Participant: A wearable prototype was worn by the first author of the paper (H. Wang) after the safety of the device was fully checked and consent was obtained. A video clip (Movie S8, Supporting Information) shows the experiment is only to demonstrate the soft coil film as a wearable sensor.

Supporting Information

Supporting Information is available from the Wiley Online Library or from the author.

Conflict of Interest

The authors declare no conflict of interest.

Keywords

flexible coils, folding and bending, soft robotics, soft sensors, wearable sensing

[1] a) H. Wang, M. Totaro, L. Beccai, *Adv. Sci.* **2018**, *5*, 1800541; b) J. C. Yang, J. Mun, S. Y. Kwon, S. Park, Z. Bao, S. Park, *Adv. Mater.* **2019**, *31*, 1904765; c) Y. Ling, T. An, L. W. Yap, B. Zhu, S. Gong, W. Cheng, *Adv. Mater.* **2019**, *32*, 1904664; d) L. Beccai, C. Lucarotti, M. Totaro, M. Taghavi, in *Soft Robotics: Trends, Applications and Challenges*, (Eds: C. Laschi, J. Rossiter, F. Iida, M. Cianchetti, L. Margheri), Springer, Cham **2017**, p. 11.

[2] a) H. Shen, *Nature* **2016**, *530*, 24; b) F. Iida, C. Laschi, *Procedia Comput. Sci.* **2011**, *7*, 99.

[3] C. D. Santangelo, *Annu. Rev. Condens. Matter Phys.* **2017**, *8*, 165.

[4] D. Rus, M. T. Tolley, *Nat. Rev. Mater.* **2018**, *3*, 101.

[5] a) S. Felton, M. Tolley, E. Demaine, D. Rus, R. J. Wood, *Science* **2014**, *345*, 644; b) M. Boyvat, J.-S. Koh, R. J. Wood, *Sci. Rob.* **2017**, *2*, eaan1544.

[6] M. Amjadi, K. U. Kyung, I. Park, M. Sitti, *Adv. Funct. Mater.* **2016**, *26*, 1678.

[7] R. K. Kramer, C. Majidi, R. Sahai, R. J. Wood, in *Proc. IEEE/RSJ International Conference on Intelligent Robots and Systems (IROS)*, **2011**, IEEE, San Francisco, CA, p. 1919.

[8] M. Totaro, T. Poliero, A. Mondini, C. Lucarotti, G. Cairoli, J. Ortiz, L. Beccai, *Sensors* **2017**, *17*, 2314.

[9] a) M. Totaro, A. Mondini, A. Bellacicca, P. Milani, L. Beccai, *Soft Rob.* **2017**, *4*, 400; b) E. L. White, J. C. Case, R. K. Kramer, *Sens. Actuators, A* **2017**, *253*, 188.

[10] H. Zhao, K. O'Brien, S. Li, R. F. Shepherd, *Sci. Rob.* **2016**, *1*, eaai7529.

[11] C. Lucarotti, M. Totaro, A. Sadeghi, B. Mazzolai, L. Beccai, *Sci. Rep.* **2015**, *5*, 8788.

[12] A. Firouzeh, J. Paik, *J. Mech. Rob.* **2015**, *7*, 021009.

[13] C. Majidi, R. Kramer, R. J. Wood, *Smart Mater. Struct.* **2011**, *20*, 105017.

[14] Y. Xiao, S. Jiang, Y. Li, W. Zhang, *Smart Mater. Struct.* **2020**, *29*, 045023.

[15] K. Wang, Z. Lou, L. Wang, L. Zhao, S. Zhao, D. Wang, W. Han, K. Jiang, G. Shen, *ACS Nano* **2019**, *13*, 9139.

[16] a) S. Ozel, N. A. Keskin, D. Khea, C. D. Onal, *Sens. Actuators, A* **2015**, *236*, 349; b) M. E. Nisser, S. M. Felton, M. T. Tolley, M. Rubenstein, R. J. Wood, in *Proc. IEEE/RSJ Int. Conf. Intelligent Robots and Systems (IROS)*, **2016**, IEEE, Daejeon, South Korea, p. 1254.

[17] H. Wang, Z. Feng, *Sens. Actuators, A* **2013**, *203*, 362.

[18] A. Sophian, G. Tian, M. Fan, *Chin. J. Mech. Eng.* **2017**, *30*, 500.

[19] a) H. Wang, J. Kow, N. Raske, G. De Boer, M. Ghajari, R. Hewson, A. Alazmani, P. Culmer, *Sens. Actuators, A* **2018**, *271*, 44; b) H. Wang, D. Jones, G. de Boer, J. Kow, L. Beccai, A. Alazmani, P. Culmer, *IEEE Sens. J.* **2018**, *18*, 7793.

[20] a) T. Kawasetsu, T. Horii, H. Ishihara, M. Asada, *IEEE Sens. J.* **2018**, *18*, 5834; b) H. Wang, M. Totaro, A. A. Blandin, L. Beccai, in *Proc. 2nd IEEE Int. Conf. Soft Robotics (RoboSoft)*, **2019**, IEEE, Seoul, South Korea, p. 242.

[21] B. Nie, R. Huang, T. Yao, Y. Zhang, Y. Miao, C. Liu, J. Liu, X. Chen, *Adv. Funct. Mater.* **2019**, *29*, 1808786.

[22] A. Fassler, C. Majidi, *Smart Mater. Struct.* **2013**, *22*, 055023.

[23] Y. Huang, W. Dong, T. Huang, Y. Wang, L. Xiao, Y. Su, Z. Yin, *Sens. Actuators, A* **2015**, *224*, 36.

[24] W. Felt, K. Y. Chin, C. D. Remy, *IEEE ASME Trans. Mechatronics* **2016**, *21*, 1201.

[25] O. Azami, D. Morisaki, T. Miyazaki, T. Kanno, K. Kawashima, *Sens. Actuators, A* **2019**, *300*, 111623.

[26] A. V. Prituja, H. Banerjee, H. Ren, *IEEE Sens. J.* **2018**, *18*, 3580.

[27] L. Y. Zhou, Q. Gao, J. F. Zhan, C. Q. Xie, J. Z. Fu, Y. He, *ACS Appl. Mater. Interfaces* **2018**, *10*, 23208.

[28] R. Herbert, S. Mishra, H. R. Lim, H. Yoo, W. H. Yeo, *Adv. Sci.* **2019**, *6*, 1901034.

[29] Z. Xie, R. Avila, Y. Huang, J. A. Rogers, *Adv. Mater.* **2020**, *32*, 1902767.

[30] M. Krivec, M. Lenzhofer, T. Moldaschl, J. Pribošek, A. Abram, M. Ortner, *Microsyst. Technol.* **2018**, *24*, 2673.

[31] H. U. Chung, B. H. Kim, J. Y. Lee, J. Lee, Z. Xie, E. M. Ibler, K. Lee, A. Banks, J. Y. Jeong, J. Kim, *Science* **2019**, *363*, eaau0780.

[32] Y. Khan, A. Thielens, S. Muin, J. Ting, C. Baumbauer, A. C. Arias, *Adv. Mater.* **2020**, *32*, 1905279.

[33] F. W. Grover, *Inductance Calculations*, Dover Publications, Mineola, New York **2009**.

[34] F. Herrault, S. Yorish, T. Crittenden, M. Allen, in *Proc. TRANSDUCERS 2009- International Solid-State Sensors, Actuators and Microsystems Conference*, **2009**, IEEE, Denver, CO p. 1718.

[35] R. Dengler, *Adv. Electromagn.* **2016**, *5*, 1.

[36] a) S. Park, N. Baugh, H. K. Shah, D. P. Parekh, I. D. Joshipura, M. D. Dickey, *Adv. Sci.* **2019**, *6*, 1901579; b) G. Scalet, *Actuators* **2020**, *9*, 10; c) E. Sachyani Keneth, G. Scalet, M. Layani, G. Tibi, A. Degani, F. Auricchio, S. Magdassi, *Soft Rob.* **2020**, *7*, 123.

[37] B. Mosadegh, P. Polygerinos, C. Keplinger, S. Wennstedt, R. F. Shepherd, U. Gupta, J. Shim, K. Bertoldi, C. J. Walsh, G. M. Whitesides, *Adv. Funct. Mater.* **2014**, *24*, 2163.

[38] Y. Lee, J. Park, A. Choe, S. Cho, J. Kim, H. Ko, *Adv. Funct. Mater.* **2020**, *30*, 1904523.

[39] J. Wang, G. Cai, S. Li, D. Gao, J. Xiong, P. S. Lee, *Adv. Mater.* **2018**, *30*, 1706157.

[40] P. Polygerinos, B. Mosadegh, A. Campo, in *Soft Robotics Toolkit*, https://softroboticstoolkit.com/book/pneunets-bending-actuator (accessed: January 15, 2020).

2000659 (13 of 13)